Implementation of a simplified method in design of hysteretic dampers for isolated highway bridges

Seyyed Behnam Golzan[a], Sébastien Langlois[b], Frederic P. Legeron[c]

ABSTRACT

Using seismic isolation systems for highway bridges modifies the structure's principal vibration modes, effectively reducing the seismic base shear conveyed from the superstructure to the substructure. However, for some low damping rubber isolation bearings, large displacements can be a problem. Supplemental hysteretic dampers can be introduced into the base-isolated bridge. This may nevertheless increase the structure base shear and the merit of adding dampers has to be evaluated properly. In this paper, a simplified method was implemented for the design of a low-cost hysteretic damper and the resulting isolator-damper system was tested experimentally. The employed design method is based on equivalent linearization approach. A full-scale elastomeric isolation bearing was characterized and used in the design of a hysteretic damper. Both the isolator and the damper went through cyclic testing and real-time dynamic substructuring (RTDS) methods to verify the capacity of the method to design base isolation-damping systems. The study was further extended to extreme seismic loading by nonlinear time history analysis. Results show that the simplified method is adequate to be used in the performance optimization of isolated-damped bridges.

Keywords: Base isolated bridge, Hysteretic damper, Real-time dynamic substructuring, Time history analysis.

[a] Eng., Ph.D., Civil Engineering Department, Université de Sherbrooke (Corresponding author); b.golzan@usherbrooke.ca
[b] Eng., Ph.D. Assistant professor, Civil Engineering Department, Université de Sherbrooke; sebastien.langlois@usherbrooke.ca
[c] Eng., Ph.D., Vice President, Bridge & Tunnel, UAE District Manager, Parsons; Frederic.Legeron@parsons.com

1. INTRODUCTION

It has been proven by Golzan and Legeron (2010) that isolation systems for small to medium span bridges can be very effective to reduce substructure loading. A drawback of the system, particularly elastomeric low damping isolation bearings, is however that the seismic displacements can be very large, resulting in expansion joints that have high initial and maintenance costs. It would be interesting to provide supplemental damping to reduce the seismic response of the structures and in particular the displacement demand. This can be achieved by high damping bearings (Naeim and Kelly 1999) or for improved stability and damping by shape memory alloy isolators (Mishra et al., 2015) or by supplementing the existing low cost isolation bearing with easy to replace dampers. Since the dampers are often sacrificial members in a structure, it is important to design elements that are economic. Such devices, nonetheless, can increase seismic loads in certain cases (Jangid and Kelly, 2001). For example Kelly (1999) has pointed out that the extra viscous dampers may increase significantly the higher-mode response in the structures. Therefore, the optimal mechanical properties of damping devices should be addressed. These properties first depend on the type of damper selected. Many types of such devices are available for designers including metallic dampers with plastic hinge mechanisms, dampers in friction, and dampers that are employing viscous properties of fluids or solid elements.

Many authors have shown that a considerable portion of the energy exerted by the earthquake can be absorbed and dissipated at designated places in a structure by yielding of metallic elements with hysteretic behavior (Moreschi and Singh, 2003). Skinner et al. (1993) showed that one method for augmenting energy dissipation of for example laminated rubber bearings, is to supplement additional components such as lead plugs inserted in the bearing. For this application, lead is advantageous compared to steel because it offers higher ductility and energy dissipation capacity in shear. This however, shall not restrict designers from employing steel dampers in different forms where deformation in flexure or even torsion is intended. Steel is easy to access and recycle, and it is also economic and durable. In a research on the effects of a steel damper on a bridge, Maleki and Bagheri (2010) showed that the steel dampers can efficiently minimize the displacement demand and the maximum stress of the superstructure of a bridge by supplying great energy dissipating capacity. Steel dampers have been reported and demonstrated efficient in the reduction of damage due to earthquake on bridge structures where there is significant deformation demands (Chen et al., 2001). Different types of steel dampers, mostly developed for building structures, which have lower deformation demands compared to bridges, include flexural deformation dampers (Stiemer et al., 1981) and (Suzuki et al., 2005), triangular dampers (Bergman and Goel, 1987) and (Pan

et al., 2014), torsional beam (Skinner et al., 1975) and U shape steel strips (Aguirre and Sánchez, 1992) and (Oh et al., 2012).

Using multi-objective optimization method Kwag and Ok (2012) proposed an optimal design approach of seismic isolation system for bridges against uncertainties in the system. In the context of small to medium span isolated highway bridges, Different objectives need to be taken into account and optimized (Hedayati and Alam, 2013) to reduce superstructure displacements. Steel hysteretic dampers may be an adequate solution for this problem. However, to facilitate its use in practice, a simplified design method is needed to identify optimal damper mechanical properties. The objective of this paper is to use a simplified design method, developed previously (Golzan et al., 2015), for the design of a steel hysteretic damper. The damper is simply composed of steel bars which are aligned horizontally. This kind of dampers is simple in fabrication and installation, economic, and easy to handle in the retrofit of existing bridges.

The following section explains the simplified method, its concept and governing equations. In section 3, the test setup designed for testing an elastomeric isolation bearing is introduced. The isolation bearing used in this study was characterized with this setup, as described in section 4. The simplified method allows estimating the required additional damping and rigidity for the structure. Then, a suitable type of damper is selected to provide the required additional damping and rigidity to the structure. In this regard, in line with the simplified method and knowing isolation bearing behavior, a steel hysteretic damper was designed, as presented in section 5. This design is performed considering a desirable rehabilitation objective for both substructure base shear and superstructure displacement. Section 6 discusses experimental procedure which encompasses two phases of testing on the isolator-damper system; 1) displacement controlled cyclic (DCC) testing and 2) real-time dynamic substructuring (RTDS) testing under seismic loading. DCC tests were used to characterize the behavior of the isolator-damper system. The RTDS tests were used to identify the response of the system under a seismic excitation, for a limited range of seismic excitation. In section 7, the properties from the first phase of experimental tests were used to develop a nonlinear time history numerical model of the isolation-damping system. The numerical model was validated with the results of the RTDS tests. Then, the numerical model was used to extend the study to extreme seismic loading.

2. Simplified design method

For bridges equipped with seismic isolators and energy dissipaters, it is usually more accurate to obtain maximum displacement demand through time-history analysis. However, in most cases of regular simple bridges (AASHTO, 2012; CSA S6-14, 2014), simple linear response spectra or uniform hazard elastic response spectra can be used at least for preliminary sizing of isolation system. These methods are based on equivalent linearization of the system by using an effective lateral stiffness and equivalent damping ratio. For most practical situations, the superstructure mass is much greater than the participant column mass, and hence the principle mode of vibration is dominated by displacements of the superstructure decoupled from the substructure by the isolation system. On this basis, in the equivalent linearized simplified design method the whole system has been simply taken as a single-degree-of-freedom model with effective stiffness and damping from both substructure and isolation system. However, bridges with tall massive columns cannot be simplified by a SDOF model.

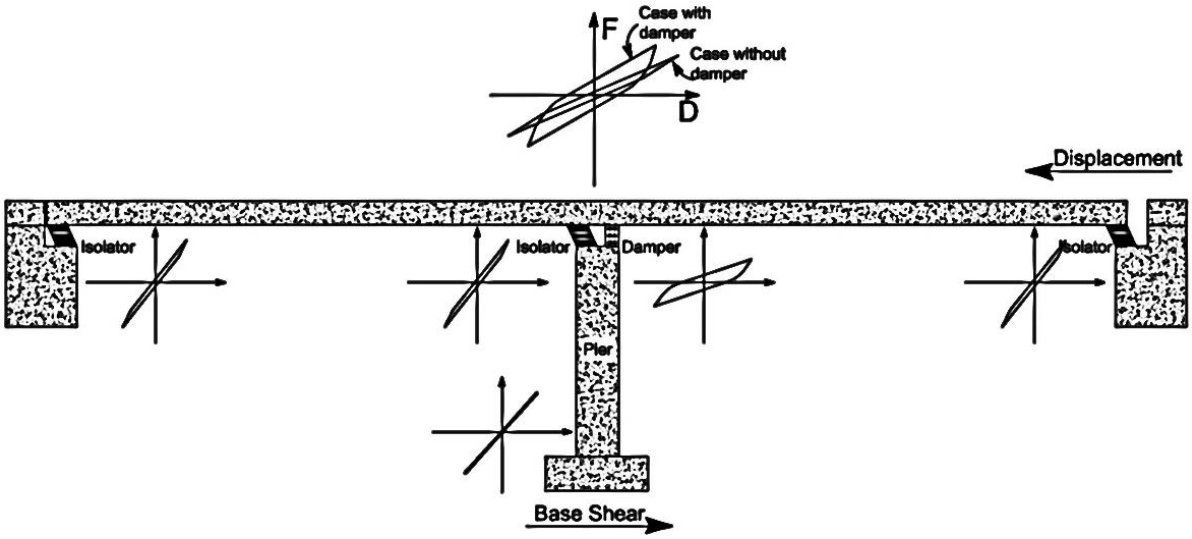

Figure 1. Isolated and damped bridge

A base isolated bridge (Figure 1) under an earthquake displaces and as a response develops base shear. The response depends on the behavior of all load supporting elements (substructure and isolation system). In certain retrofitting cases, a damper is added to this system to moderate its response in terms of displacement and base shear. As shown in Figure 1, the case without damper provides low damping. This can be seen for example in some of low damping elastomeric isolation bearings. Golzan et al. (2015) proposed a simplified method for the retrofit of simple regular bridges. The method is based on the equivalent linearization of the bridge elements and provides required added design stiffness and damping for a particular isolated bridge to attain a desired response

94 under seismic loadings. The method restrains the parameters for the added damper such that the variation in the
95 base shear ($\varepsilon=(F_2-F_1)/F_1$) and the reduced displacement variation ($\varphi=(D_2-D_1)/D_1$) remain within the required
96 range. For a range of damping reduction factor after and before retrofit (B_2/B_1) between 1 and $(1-\varphi)^{-1}$, the
97 two equations for damping and stiffness from Golzan et al. (2015) are:
98

$$\frac{T_{e_1}}{T_{e_2}} = \frac{B_2}{B_1} = [(1-\varphi)(1+\varepsilon)]^{-\frac{1}{2}} \quad \text{Equation 1}$$

$$\frac{K_{eff_2}}{K_{eff_1}} = \left(\frac{T_{e_1}}{T_{e_2}}\right)^2 = \frac{1+\varepsilon}{1-\varphi} \quad \text{Equation 2}$$

99 Where, T_e is the natural period of the structure. Identifying target values for B_2 and K_{eff2} allows calculating
100 the stiffness and damping design values for the damper. For the configuration studied, the isolation bearing and
101 the damper specimens are aligned in parallel. Final equivalent damping ratio in Equation 3 comes from the
102 participation of damping from both segments proportional to the ratio of stiffness of each to the combined
103 effective stiffness for two parallel springs in Equation 4 (Roesset et al., 1973; Jara and Casas, 2006).

$$\xi_2 = \frac{K_i}{K_i + K_d}\xi_i + \frac{K_d}{K_i + K_d}\xi_d \quad \text{Equation 3}$$

$$K_{eff2} = K_i + K_d \quad \text{Equation 4}$$

104 Where, ξ_i, k_i, ξ_d and k_d are the damping ratios and stiffnesses attributed to isolator and damper respectively.

105 ## 3. Experimental setup

106 This section describes the equipment used to perform the tests on the full size bearing isolator device and the
107 proposed damper. The test setup, shown in Figure 2, was initially designed to perform tests on isolation bearing
108 devices. It allows to apply a constant vertical load and to impose a horizontal displacement on the isolation
109 bearing. The test setup was modified to add a damper prototype in parallel to the isolator. The testing procedure
110 is monitored by a data acquisition and a controlling system. The controller is governed by a commercial software
111 which is connected to the actuators through a signal channel.
112 The various parts of the test setup are: the vertical and horizontal loading system; the rollers sliding surface; the
113 instruments to measure displacements; and the control systems.
114

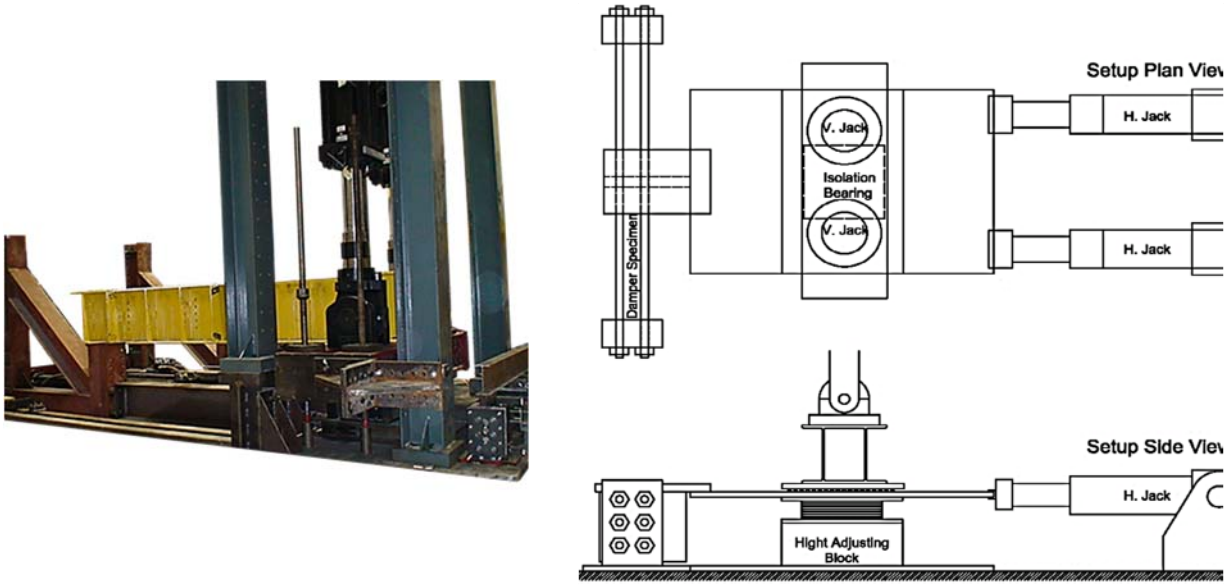

Figure 2. Test setup for isolation bearing and damper

To simulate the gravity load of the bridge deck on the isolation system, it is important to have a system that imposes a constant vertical load. The vertical load is applied by two servo-controlled hydraulic jacks that have a nominal capacity of 1000kN. These two servo-controlled jacks are fixed to the overhead frame and are supporting the weight of the test setup that otherwise should rest on the bearing isolator device. The resultant load is concentric because the two jacks are symmetrically arranged with regard to the isolation bearing center and, it is considered uniformly distributed due to the plates and the beams of the vertical load system. During horizontal displacement, the rotation of the vertical loading system is prevented by a beam fixed at this system at one extremity and pinned at the other one (Figure 2). This beam also prevents longitudinal movement of the vertical load. Transverse movement of the vertical load was prevented with a guiding device that allows vertical displacement.

The horizontal load is applied by a pair of servo-controlled hydraulic jacks of a nominal capacity of 250kN and a total shaft extension of 1000 mm (±500 mm). The upper plate of the isolation bearing is bounded to the horizontal jacks by the mobile plate, whereas the lower plate of the isolation bearing is fixed to the ground plate. The anchorage box-beam supporting the fixed end of the horizontal jacks is connected to the ground plate by beams that can resist the horizontal force applied by the jacks. Furthermore, the anchorage box-beam and the ground plate are attached to the structural strong-floor of the laboratory to obtain a maximum of rigidity of the test setup. The applied horizontal load is displacement controlled and is measured directly by the jacks applying

the load. In the characterization phase of the isolation bearing, the damper is not installed in its place so that the whole horizontal force is carried by the bearing.

The required decoupling and sliding surface between the upper plate and the vertical load system is accomplished by a set of parallel rollers fixed in a steel frame (Figure 3a&b). The resistance in displacement of clean rollers under a vertical load of 900kN is about 6.3kN which represents 0.7% of the vertical load. Thus the total measured force includes a resistance caused by the friction of the roller and the sliding plates which should be deducted.

(a) (b)

Figure 3. Roller between vertical jacks and the sliding plate over the bearing (a & b); Isolation bearing (b)

The horizontal displacements are measured by diverse devices. The extension of the two horizontal jacks establishes the main measure of the horizontal displacement. However, the extension of the jacks can differ from what is measured at the level of the plates of the isolation bearing because of the stiffness of the assembly. Thus two sensors measure the displacement of the upper and lower plates in the center of the isolation bearing relative to the ground plate. The relative horizontal displacement of the plates of the isolation bearing is then obtained by subtraction. The difference between the displacement measured by the sensors and the horizontal jacks can reach up to 5 mm.

The forces and displacements are recorded at the rate of 25 Hz for cyclic tests and 100 Hz for real time hybrid tests by the controller of the jacks. The acquisition of the data begins before the application of the vertical load and ends after it has been removed. One MTS controller operates the servo-valve of each of the four hydraulic jacks (2 vertical and 2 horizontal) independently from the force or displacement feedback, at the choice of the operator.

4. Characterizing the isolation bearing

Before designing the damper, it is necessary to perform comprehensive testing in order to characterize the isolation bearing to find out its displacement dependant nonlinear properties. This bearing is a laminated rubber isolation bearing designed for one of the piers of a highway bridge in the province of Quebec, Canada. It was designed for a vertical load of 900kN, a horizontal force of 302kN and a maximum design displacement of 103mm. Two series of characterization tests were performed on the isolation bearing in Figure 3: one before testing with dampers and the second as a control series after testing with dampers. No significant change was noticed in the behavior of the isolator after all tests.

The characterization test on the bearing was performed using a progressive sinusoidal loading as specified by CSA S6 (2006). Testing the bearing at different displacements and drawing the trend line for all captured data, Figure 4 shows how the effective stiffness and the equivalent viscous damping ratio vary at various displacements of the bearing. Based on this characterization, some constituting laws of the isolator were drawn to constitute an approximate bilinear model of the bearing in the design of the damper.

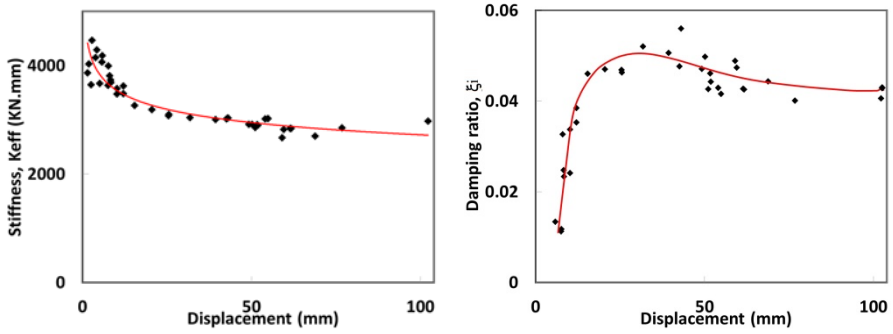

Figure 4. Behavior of the bearing at different displacements

From Figure 4, the effective stiffness and the equivalent damping ratio of the isolator at design displacement of 103 mm are 2940kN/m and 0.045 respectively. The test condition simulates an isolator on a bridge with a very stiff substructure (Base of the lab) that can be assumed infinitely rigid. Considering the design vertical load of 900kN on the isolator, the natural period of the system is equal to 1.1s.

5. Designing a hysteretic damper

In the following sections, a system combining a base isolation bearing and a damper will be designed and tested. This system provides a complete example of an application of the simplified method.

To facilitate its use in the design of isolated bridges, dampers need to be simple, low maintenance, and easy to procure. For these reasons, the use of a hysteretic damper made of steel bars is proposed. However, because metallic dampers have a certain intrinsic stiffness, they could produce an increase in force depending on the post elastic characteristics of the damper which greatly governs its damping level.

The proposed damper in this paper is composed of several fixed end steel bars aligned horizontally (Figure 5a) that dissipate the energy of a vibration by plastic hinge mechanisms at both ends and mid-length of the bars (Figure 5b). The response of the superstructure to earthquake in terms of exerted force is applied to the damper bars through an articulation which assures the yielding of the bars in bending only and not in torsion. The number of bars and their lengths as well as the steel grade can determine to what extent the displacement demand will be attended by this design method. The choice of several bars is useful for distributing the end moments on a larger surface.

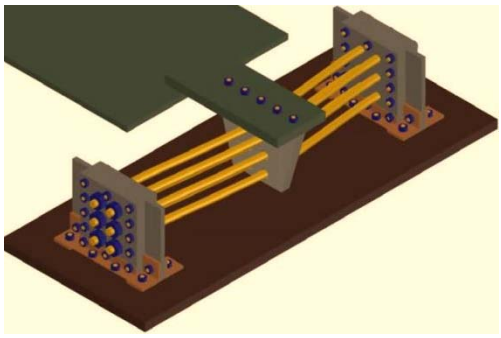

(a)

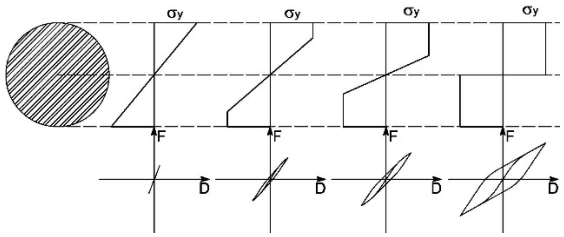

(b)

Figure 5. Conceptual configuration of the damper (a); Energy dissipation on plastic cross section (b)

The horizontal disposition of the elements versus the vertical disposition is a simple way to ensure that a temporary or permanent vertical displacement of the bridge will not impose undesirable axial forces in the damper. This configuration will only leave a small bending moment on the bars in the vertical direction. Furthermore, this configuration gives more flexibility in the choice of number, length and diameter of the bars. However, this type of damper will perform in one direction, and therefore, horizontal bars would need to be placed in any direction of the bridge subject to retrofit. The middle plate that transfers the horizontal displacement of the upper plate to the specimen is not fixed to the bars so that the bars can freely rotate and slightly move in

the length of the bars and avoid any torsion or axial loads imposed by bidirectional movement of the middle plate.

To use the simplified method as summarized in Section 2 and detailed in Golzan et al. (2015), a simple model needs to characterize the stiffness and damping behaviour of both isolators and dampers. The AASHTO provisions specify an equivalent linearization of the isolation bearing based on the bilinear model (AASHTO, 2010). Hwang et al., (1996) proposed that to obtain the effective stiffness K_{eff} and equivalent damping of a hysteretic system ξ_{eq}, three parameters of elastic stiffness (K_{el}), post yield stiffness ratio ($\alpha = K_{el} / K_{pl}$) and ductility ratio ($\mu = D/D_y$ where D_y is the yield displacement) could be taken as variables and set to desirable values. Equation 5 shows the value of effective stiffness in a bilinear hysteresis model and Equation 6 shows the equivalent damping in the same model. These equations were formulated for isolators, but they can also be applied for the evaluation of damper properties.

$$K_e = \frac{1 + \alpha(\mu - 1)}{\mu} k_{el} \qquad \text{Equation 5}$$

$$\xi_e = \frac{2(1 - \alpha)(1 - \frac{1}{\mu})}{\pi[1 + \alpha(\mu - 1)]} \qquad \text{Equation 6}$$

Assuming the desired equilibrated displacement and force for the combination of isolation bearing and damper, the geometry of the damper can be determined based on Equations 7&8 for round steel bars subject to bending:

$$K_{el} = \frac{3n\pi d^4 E}{l^3} \qquad \text{Equation 7}$$

$$D_y = \frac{F_y . l^2}{12E . d} \qquad \text{Equation 8}$$

Where, n is the number of steel bars, l is the length of the bars, d is the diameter of the bars and E is the modulus of elasticity (equal to 200 GPa). D_y and F_y are respectively the yield displacement and strength of the steel bars in bending.

The first step in the design of the damper is to set targets for variation in base shear ε, and variation in superstructure displacement φ. In the present case, the (ε%, φ%) scenario was taken arbitrarily (0, -50). From Equation 1, the target damping ξ_2 is found to be 0.08 and from Equation 2 the target effective stiffness K_{eff2} equals to 5880kN/m for the complete structure. The effective stiffness of the damper K_d, from Equation 4 is 2940kN and its equivalent damping ratio ξ_d from Equation 3 is 0.14.

The second step is to set the stiffness K_e and damping ξ_e in Equation 5&6 equal to K_d, and ξ_d respectively and then calculate the parameters for the representation of the damper in the bilinear model. Two commercially available steel grades with the approximate yield strength F_y of 350MPa (hot-rolled steel) and 580MPa (cold-rolled steel) were chosen. Having performed some preliminary tests, the post yield stiffness ratios were taken approximate values of 0.3 and 0.4 for hot-rolled and cold-rolled steel respectively. This ratio depends on both the steel properties and the geometry of the damper. Ductility ratio ($\mu=D/D_y$ where D is already defined with the target variation in displacement φ) and elastic stiffness K_{el} can then be calculated using Equations 5&6. In the third step, the elastic stiffness K_{el} and the elastic displacement D_y can be related to the geometry of the damper using Equations 7&8. The number of bars n needs to be assumed in order to solve for the diameter and length of the bars, In this case, the use of six bars was found to give practical bar sizes for the available test setup and isolator. For the damper composed of six bars, the diameter and length of bars were found respectively equal to 36mm and 1352mm for hot-rolled steel and 35mm and 1499mm for cold-rolled steel. For practical reasons, it was decided to use bars of 38mm (1.5 inches) diameter and the 1500mm length for both hot rolled and cold-rolled steel. A total of five specimens were fabricated to be tested: three specimens made up of cold-rolled steel (CR) and two specimens made up of hot-rolled (HR) steel. For each specimen, two coupons were tested according to ASTM E8 / E8M - 15a (2015) standard test methods for tension testing of metallic materials to determine the steel yield strength F_y.

With the selected values for n, d, l and the measured values for F_y, the actual properties of stiffness and damping of the damper can be predicted by Equations 5&6. Subsequently, the final stiffness and damping properties of the combined isolation-damping system can be calculated with Equations 3&4. This leads to updated predictions for (ε%, φ%), as calculated with Equations 1&2, which can be a little different from the primarily assumed ones. Values found using the procedure above for the selected test specimens are summarized in Table 1.

Table 1. Design properties

Specimen	F_y(MPa)	D_y(mm)	ξ_2	K_{eff2}	(ε%, φ%)	D (mm)
HR1	371	9	0.11	5998	(-7, -54)	47
HR2	356	9	0.10	6015	(-6, -54)	47
CR1	590	14	0.11	7227	(3, -58)	43

CR2	596	15	0.10	7472	(6, -58)	43
CR3	530	13	0.09	7301	(9, -56)	45

6. Testing isolation bearing and dampers

Two testing procedures were used in this phase: displacement controlled cyclic (DCC) testing and real-time dynamic substructuring (RTDS) testing. For a complete fixation of the bars by the end block against any rotational and translational displacement a girder was added (Figure 6b) on top of the blocks to provide ideal fixed boundary conditions. As shown in Figure 6, a laser sensor (on the vertical bar) was placed to measure the horizontal displacement in the middle of the specimen relative to the end blocks.

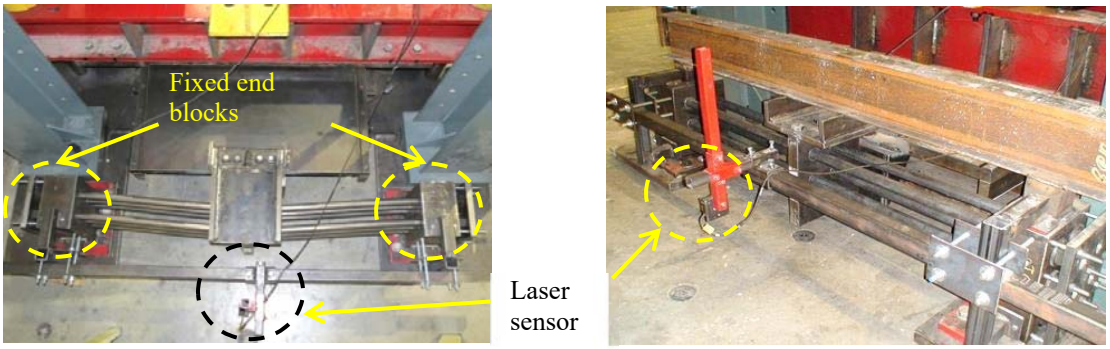

(a) (b)

Figure 6. Plan view of the damper without girder (a); Fixing girder between blocks (b)

6.1 Displacement controlled cyclic (DCC) tests

Displacement controlled cyclic loading has been performed on all specimens. These tests for specimens HR2 and CR3 were performed after RTDS testing. Frequency of loading and number of cycles were two parameters to be verified during the tests. A frequency of 0.25 Hz was used in general for DCC tests, but tests were also performed at 0.1 Hz and 0.5 Hz. The effect of loading frequency on the results of displacement controlled cyclic testing was found to be negligible.

To match approximately the final displacements outlined in Table 1, the specimens were tested at three or four amplitudes with the lowest amplitude corresponding approximately to yield displacement. These displacement amplitudes are 9, 50, and 60 mm for hot rolled specimens and 12, 30, 40, and 50 mm for cold rolled specimens. Three cycles at each displacement amplitude were performed consecutively as shown in the loading

force and hysteretic curves of Figure 7 for specimens HR1 and CR2. In this figure, force for isolator alone and for combined isolator and damper has been measured in two different tests.

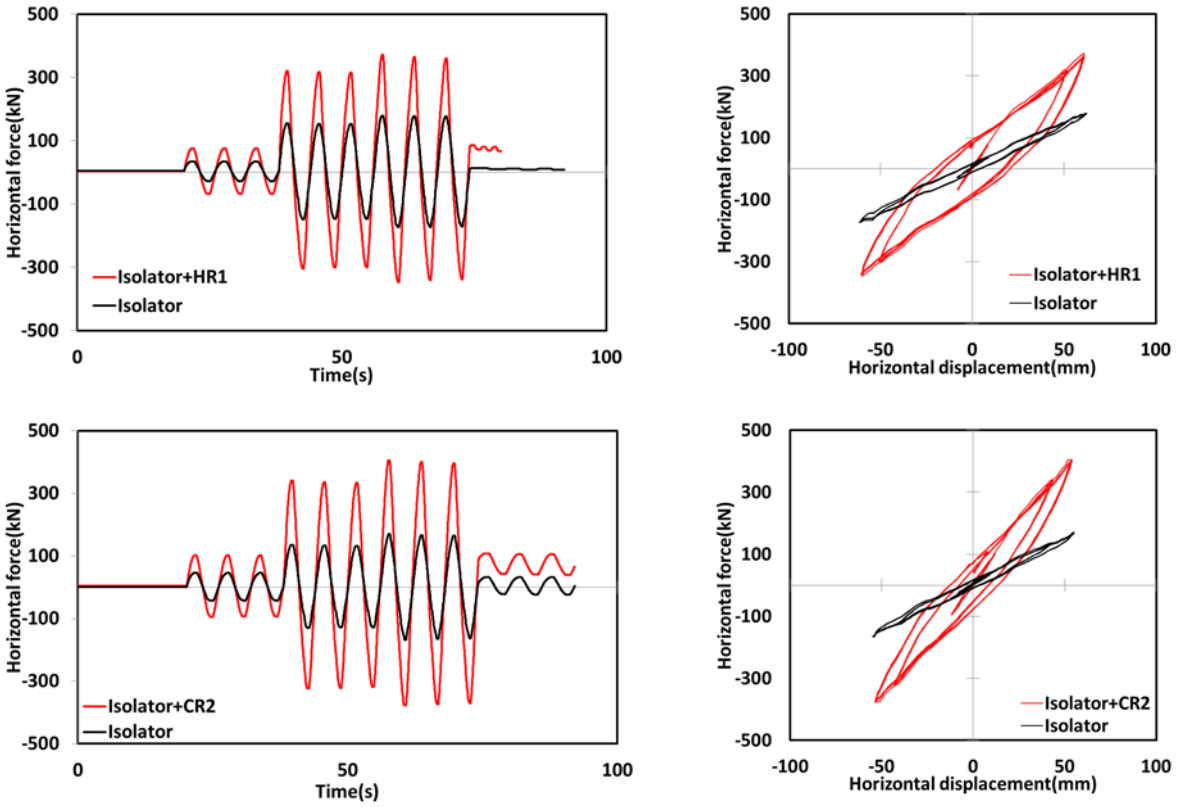

Figure 7. Comparison of the combined system vs. isolation only for two specimens

As shown in Figure 7, hot rolled steel dampers are more advantageous with lower added stiffness and more damping effect compared to cold rolled steel dampers; having lower yield displacement, they also reach larger ductility values. In specimens HR1 and HR2, the attained ductility ratio at the maximum design displacement of the specimens is 5.2 and for CR1 through CR3 they are 3.1, 2.9 and 3.5 respectively. A comparison in terms of effective stiffness and equivalent damping has been made between the isolation bearing and its combination with five specimens in Figure 8. While specimens HR1, CR1 and CR2 were first tested by DCC method, it should be noted that the specimens HR2 and CR3 underwent real time dynamic substructuring (RTDS) tests as discussed in section 6.2. It is seen in Figure 8 that being damaged by RTDS tests (Passing yield displacement limit of the specimen) does not have a significant effect on the effective stiffness and equivalent damping ratio of the combined system because the displacement after yield in RTDS tests is much less than the designated displacements in cyclic tests. It is also seen in this figure that for a given displacement, hot rolled steel specimens have a higher damping ratio.

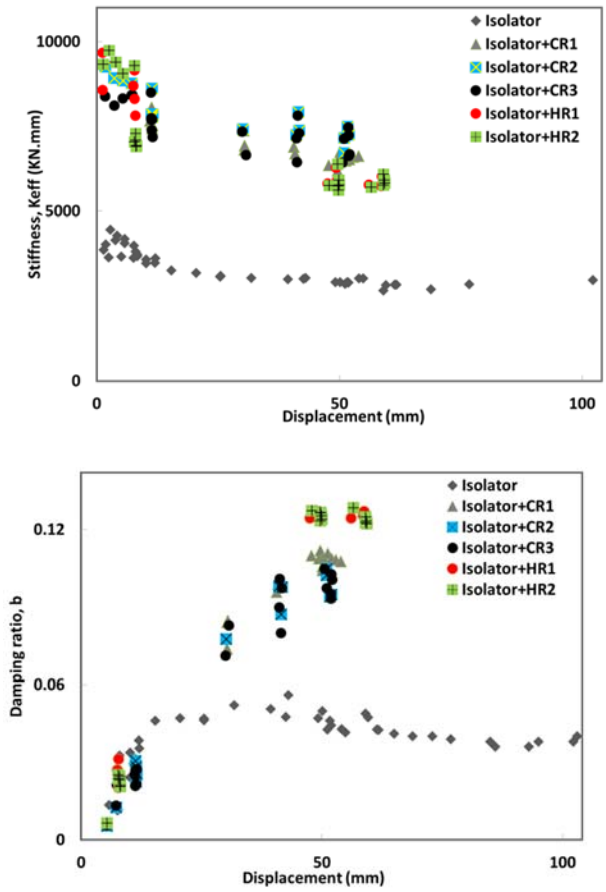

Figure 8. Effective stiffness and equivalent damping ratio of specimens at various displacements

6.2 Real-time dynamic substructuring (RTDS) tests

The method of RTDS testing, often referred to as real-time hybrid testing, combines a numerical model with an experimental test. By substructuring techniques, it is possible to experimentally test only one part of a structure and subsequently study the global behavior of it in real time.

For a known external excitation and employing a proper integration algorithm, the response of the structure could be solved numerically at any time step for the relevant displacement command applied by a hydraulic actuator. The acquired substructures' restoring forces are subsequently entered into the integration algorithm for the next time step displacement command.

Let's assume a bridge deck with a known mass placed on top of an isolation system as described in this study (section 4) with a very stiff pier (solid floor slab of the laboratory). The system is equipped with the above-mentioned damper parallel with the isolator. Considering that the movement of the bridge during an earthquake takes place essentially in the horizontal direction at the level of the isolation bearing, the structure can be

simplified as a single degree of freedom (SDOF) system. Since the effect of rollers is small and the base of the setup can be assumed to be completely rigid, the equation of motion can be written as:

$$m_{deck}\ddot{x} + c_{i+d}\dot{x} + k_{eff}x = F(t)_{seism} \quad \text{Equation 9}$$

Where m_{deck}, is the mass of the deck taken as 91.7 tons, k_{eff} is the effective stiffness of the combined system, c_{i+d} is the damping from the combined system, and $\ddot{x}$, $\dot{x}$, x are acceleration, velocity and displacement of the system respectively. By considering the deck mass which is applied virtually and applying the external earthquake loading on the system, the response of the combined experimental and numerical structure can be determined in real time by RTDS testing method. The effective stiffness and equivalent damping behavior of the experimental portion leads to restoring force used by the system to calculate the global response in a stepwise manner.

Figure 9 (a) is a schematic SDOF view of a bridge on an isolation bearing and a damper. The numerical part is composed of only the deck mass while the bearing system is experimentally tested. As shown in Figure 9 (b), actuators are directed by an industrial MTS controller (Flextest) rhythmed at every 1/1024 s. The MTS controller is commanded itself by a National Instruments controller (CompactRIO) (Figure 9c). This latter controller resolves in real time the equation of movement by Rosenbrock-W direct integration scheme (Lamarche et al. 2009) with a rhythm of 2.5 milliseconds. Both controllers communicate the signals of force-displacement by analog channels.

In real time, a particular attention should be paid to the control of delay between the command for displacement and the movement of the jack. For these tests, the delay was corrected by adding of a straight feedforward gain to the controller.

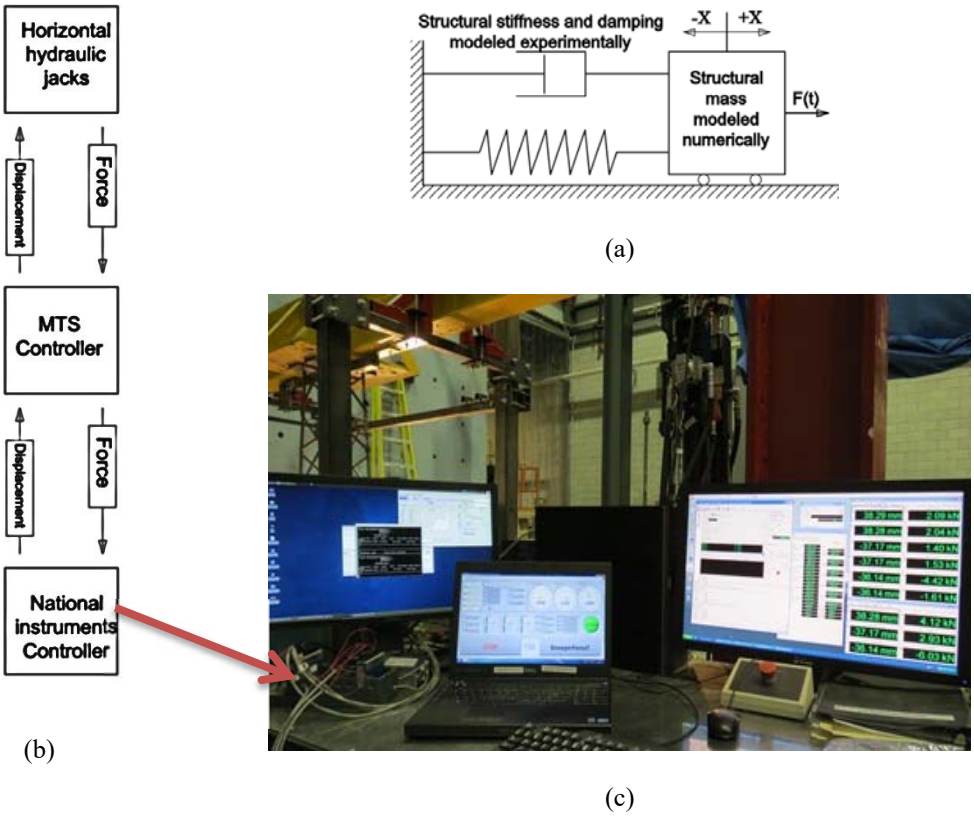

Figure 9. Configuration for RTDS testing on a SDOF model

Real time hybrid tests were done on isolator alone, undamaged bars (CR3 & HR2) and damaged bars from cyclic tests (CR2 & HR1). Northridge earthquake accelerograms scaled at 10%, 20%, and 30% of its ground acceleration were used for these tests. Scaled accelerograms were taken as input to National Instruments controller and subsequently to MTS controller which commands the horizontal jacks. Due to velocity limitation of the horizontal hydraulic jacks for displacements over 40 mm with the velocity of 210 mm/s, the scaled accelerograms to 40% on isolator alone was not performed and hence the comparison of the results for this case with the specimens is not possible. Furthermore, the test would abort near the maximum peak point of the velocity where the jacks could not follow the command from the controller.

Using RTDS tests has the advantage of not imposing the displacement or the force on the system: it is the seismic excitation that is controlled. Figure 10 shows the displacement and force history of two specimens exposed to Northridge earthquake scaled to 30%. For both the hot rolled (HR1) and cold rolled (CR3) specimens presented, a decrease in displacement and an increase of the force is obtained by adding the damper to the system.

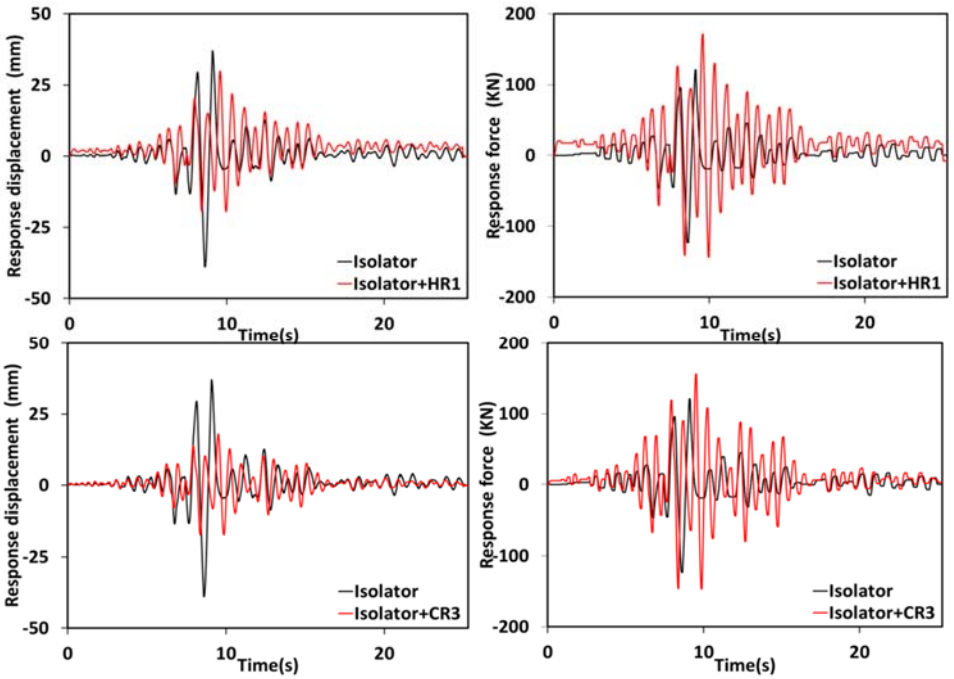

Figure 10.Displacement and force history of HR1 and CR3 with and without isolator under Northridge 30%

Hysteretic behavior of the two specimens, as shown in Figure 11, shows the effect of steel grade on the damping and stiffness under the same earthquake. It is seen that the cold rolled specimen shows higher stiffness and lower damping, and hence higher response force compared to the hot rolled specimen.

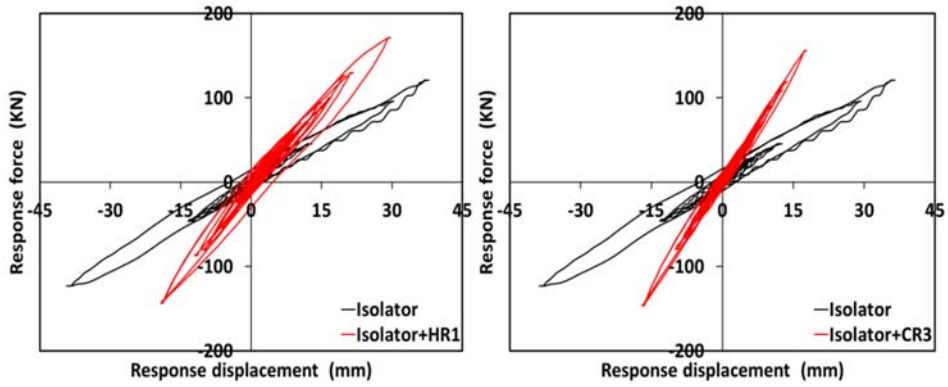

Figure 11. Hysteretic response of HR1& CR3 with and without isolator under Northridge 30%

All RTDS testing results for specimens HR1, HR2, CR2 and CR3 under Northridge scaled to 30% are summarized in Table 2 which shows the effective values of damping and stiffness at the displacements obtained. It also shows the values of increase in the force (ε) and decrease in the displacement (φ) relative to the case where the isolation bearing was tested. Specimens HR1 and CR2 have already been tested by DCC method at amplitudes of 47mm and 43mm respectively. This implies that the specimens have yielded and in RTDS tests can show

different behavior from other two specimens. Under the same accelerograms, they represent lower displacement and force with more effective stiffness and low damping ratio.

Table 2. RTDS testing results for specimens under Northridge scaled to 30%

	$D_{min/max}$	$F_{min/max}$	μ	K_{eff}	φ%	ε%	ξ%
Isolator	-38.8 36.5	-123.1 121	- -	3242	-	-	5.5
HR1	-17.3 26.5	-143.5 171.2	1.92 2.94	7183	-42	+29	7.3
HR2 (RTDS first)	-15.4 15.4	-130.4 144.7	1.71 1.71	8938	-59	+13	4.1
CR2	-16.3 22	-136.4 167.6	1.09 1.47	7924	-49	+25	4.4
CR3 (RTDS first)	-17.1 17.8	-146.5 156	1.32 1.37	8668	-54	+24	3.3

For 30% of Northridge, all specimens experience yielding as their displacements are greater than their respective yielding limit. From the results, the ratio of damping reduction coefficients for the combined cases, B_2, and the case with isolation bearing, B_1, except for HR1 is less than 1 which is contrary to the assumption that B_2/B_1 should be between 1 and $(1-\varphi)^{-1}$. This is attributed to the fact that tests with higher scales of Northridge were not possible due to the speed limitations. Nevertheless, for specimen HR1, the ratio of B_2/B_1 is calculated by Equation 1 of the method to be 1.15 while this ratio from the tests is 1.09 which shows a close conformity between the tests and the method. It is expected that for higher displacements, the contribution of the damper to the overall damping of the system will increase significantly.

The ratio of effective stiffness from combined system to isolator, K_{eff2}/K_{eff1} based on Equation 2 of the method shows a close match between the test results and the estimations by the method. In summary, the stiffness obtained in the RTDS tests for combined isolator and damper was similar to those predicted by the simplified method. However, due to limitations in the actuator's speed, these tests could not reach amplitudes for which the dampers exhibit the damping ratios calculated with the simplified approach.

7. Extending study with numerical modelling

A 2D numerical model of the setup was analysed in the finite element software SAP2000 to first reproduce some of the RTDS tests, and then extend the study to excitation levels for which the damper was designed. As it is shown in Figure 12a, the model consists of three main components of the test setup. To model the isolation system, a biaxial hysteretic link element was employed. It couples plasticity properties for the two shear deformations, and linear effective stiffness properties for the other four deformations. The plasticity model is based on the hysteretic behavior proposed by Park et al. (1986). The vertical property of the isolator was taken linear under the dead and service loads. For nonlinear direct integration time history, mass and stiffness proportional damping was set to zero for all cases of the model. For time integration parameters, Hilber-Hughes-Taylor method was used. A bilinear model following Equations 3 and 4 was assumed to define the nonlinear properties of the isolator. Based on the characterization tests presented in Section 4, the properties of the bilinear model for the isolator were found to be D_y = 13mm, K_{el}=3900 and α=0.72.

To model the damper and also the friction of the roller, a Wen plasticity property was defined. For this link element, we can specify independent uniaxial plasticity properties for each deformational degree of freedom; all internal deformations are independent and yielding at one degree of freedom may not affect the behavior of the other deformations. The damper element in the model is not subject to vertical loading under gravity, whereas the roller element is subject to a load of 900kN. In order to define the properties of the bilinear model for the damper, Equations 3 and 4 are also used. The elastic displacement D_y and stiffness K_{el} were assumed equal to the calculated values from Equations 6 and 7. The post yield stiffness ratio, α, was evaluated by subtracting the force-displacement curve from tests on the isolator alone (section 4) from the force-displacement curve for the combined system (section 6.1). For hot rolled and cold rolled specimens, α, was evaluated on average as 0.27 and 0.42 respectively.

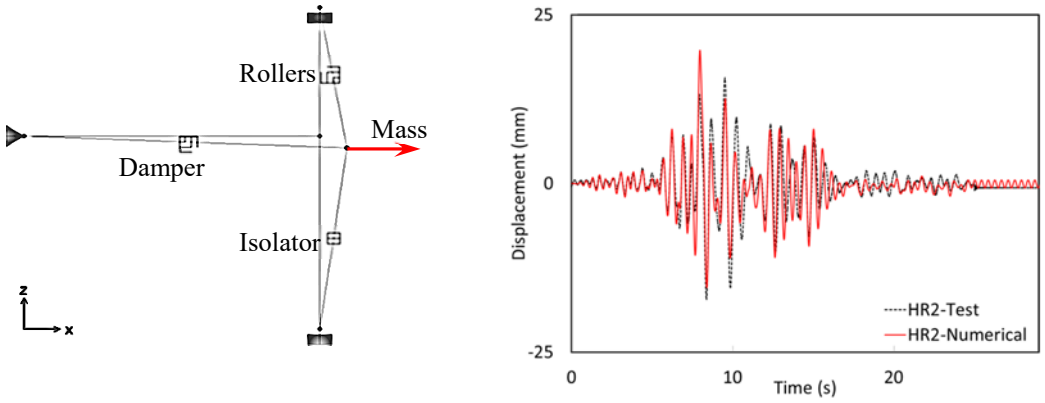

(a) (b)

Figure 12. Numerical model (a); Test& analysis comparison under Northridge 30%

Figure 12b compares the history of displacement from analysis and RTDS testing for HR2. It is shown that the displacement time history from both tests and numerical analyses matches closely.

In order for further extending the study, six synthetic near fault and far from fault ground motion time histories (Atkinson et al., 2015) best matching between 0.5 s to 2 s of the period for Montreal and Sherbrooke soil type C, have been used to evaluate the behavior of the structure. Three of six accelerograms were taken for Montreal (east7c1-28, east6c1-30 & east6c1-42) and the other three were taken for Sherbrooke (east6c1-30, east7c1-42 & east6c1-42). Each earthquake name refers to region, magnitude, site class and distance. Thus east6c1 has the accelerograms for the east for M6.0, on site class C, for distances 10-15 km. Records for both magnitudes of 6.0 and 7.0 for the east have been taken. Numbers at the end of the name refer to the number of the earthquake in the sets of 45 records. Each accelerograms was scaled so that the numerical model without the damper yielded approximately maximum design response of the bearing. Subsequently the same scaled earthquake was applied to the model with the damper element to verify the rate of decrease in displacement as well as the rate of increase in the base shear of the model. Since the specimens with the same grade of steel had similar results, they were regrouped into only HR and CR numerical models. Figure 13 shows the history of response for isolator with and without HR specimens.

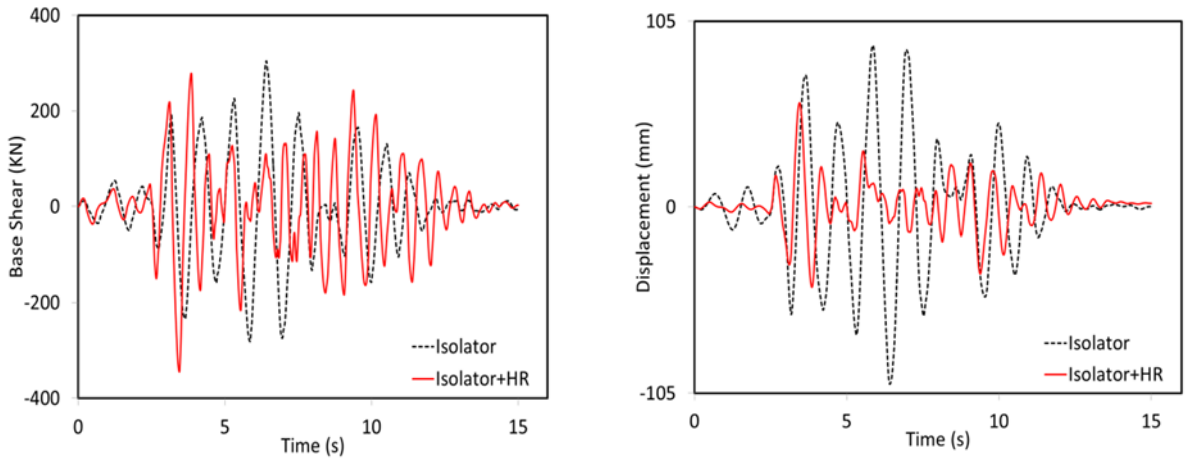

(a) (b)

Figure 13. Numerical results for specimens under design accelerograms of scaled east7c1_28

The average values of response of the system without and with dampers under six accelerograms are compared to the results from the simplified method in Table 3.

Table 3.Response of the combined system for the numerical model

	Simplified method		DCC testing	Numerical method extended from RTDS	
Specimen	D(mm) (**φ**)	F (kN) (**ε**)	F(kN) (**ε**)	D(mm) (**φ**)	F (kN) (**ε**)
HR1	47 (-54%)	284(-7%)	297 (-2%)	56 (-42%)	326(11%)
HR2	47 (-54%)	285(-6%)	303 (0%)		
CR1	43 (-58%)	313 (3%)	334 (10%)	52 (-47%)	370(26%)
CR2	43 (-58%)	323 (6%)	335 (11%)		

CR3	45 (-56%)	331 (9%)	335 (11%)

Although the variations in displacement and base shear have a general agreement between the numerical model and the simplified method, it is observed that the decrease in displacement is lower and the increase in base shear is higher for the numerical model. The variations in the force and displacement response from the time history analysis can be different from what has been predicted by the simplified method and DCC testing because the proposed method simply assumes that the response is inversely proportional to the period.

Although mild steel (HR) shows more desirable behavior, the increased force due to increased effective stiffness under inertial loading on the system is still present. By increased effective stiffness the fundamental period of the combined system will decrease as well. On a real bridge structure, based on the design goals and features of the structure and the damper, the increased stiffness can be handled without raising efforts while behavioral and economic advantages of the system should be verified by the designer. It should also be noted that the original non-isolated system must be compared to the isolated-damped structure. The proposed method and system would be interesting if overall efforts are lower to what would have been obtained on a conventional non-isolated structure, and that the movements are similar. In case of a damage subsequent to a sever seismic event the replacement of the proposed system can be relatively easy compared to the repair of a bridge pier and/or its foundation. Eventually, the simplified method can be a useful tool for the rapid selection of damper properties to reduce isolated bridge displacements under seismic loads.

8. Concluding remarks

A simplified method for the design and retrofit of energy dissipating systems for highway bridges has been presented. Following this simplified method, very simple and easy-to-replace steel hysteretic dampers prototypes have been designed and tested under DCC and RTDS testing. After the experimental verifications, the behavior of the proposed damper was further investigated numerically.

The main conclusions are as follows:

1. The simplified method can be useful in selecting the optimal added stiffness and damping to a structure where the control of displacement and base shear is required.

2.A simple steel hysteric damper has been designed that has several advantages. First the elements are horizontal so the vertical movements of the deck of the bridge may not affect its functionality. It also permits to choose a desired length and cross section for the damper elements. Finally, the three point plastic hinge mechanism in the proposed damper offers a greater capacity for the elements to dissipate earthquake energy.

3.DCC test results for both hot rolled and cold rolled specimens show a good conformity between the predictions of the method and the test results. Hot rolled specimens show more damping and reach higher values of plastic deformation compared to the cold rolled ones.

4.RTDS testing results for HR1 specimen show a close conformity between the method and the tests in terms of added stiffness. However, due to velocity limitations of the hydraulic jacks for other specimens, damping ratio stayed lower than the case with the isolator alone because the damper could not dissipate much energy for these low amplitude cycles.

5.Results from nonlinear time history analyses of the specimens follows closely the history recorded during the RTDS tests.

6.The extended numerical modeling depicts a general agreement between the simplified method and test results on prototypes. The time history analysis on average predicts a smaller decrease in displacement and a larger increase in base shear.

7.The damper developed in this study is only one suggestion to implement the simplified method in practice. Other existing dampers could be tested for a better verification of the method.

ACKNOWLEDGMENTS

This research is part of the Canadian Seismic Research Network. The authors gratefully acknowledge the financial support of the Natural Sciences and Engineering Research Council of Canada under the strategic Research Networks program. The authors also cordially appreciate the kind contributions of Marc Demers and Alex Loignon in realizing the experiments and consequently reviewing and editing the manuscript.

REFERENCES

AASHTO (The American Association of State Highway and Transportation Officials). (2010). “Guide Specifications for Seismic Isolation Design”, 3rd Ed., Washington, DC.

444 Aguirre, M. and Sánchez, A. R., (1992). “Structural Seismic Damper,” Journal of Structural Engineering, 118, 1158-
445 1171.
446 ASTM (American Society for Testing and Materials). (2015). “Standard Test Methods for Tension Testing of
447 Metallic Materials.” E8 / E8M - 15a, West Conshohocken, PA.
448 Atkinson, G., Assatourians, K. and Dunn, B. Engineering Seismology Toolbox. Available from
449 www.seismotoolbox.ca.
450 Bergman, D. M. and Goel, S. C., (1987). “Evaluation of Cyclic Testing of Steel-Plate Devices for Added Damping
451 and Stiffness,” Report No. UMCE 87-10, University of Michigan, Ann Harbor, MI.
452 Chen G., Mu H. and Bothe E.R. (2001). Metallic Dampers for Seismic Design and Retrofit of Bridges, Final report
453 RDT 01-005, University of Missouri-Rolla
454 CAN/CSA-S6 (Canadian Standards Association). (2006). “Canadian National Highway Bridge Design Code;
455 Canada.” Mississauga, ON, Canada.
456 CSI (Computers and structures Inc.) (2015). “Analysis Reference Manual for SAP2000 , ETABS, SAFE and
457 CSiBridge.” Berkeley, CA.
458 Hedayati Dezfuli F, Alam MS. (2013). “Multi-criteria optimization and seismic perfor-mance assessment of carbon
459 FRP-based elastomeric isolator.” Engineering Structures, 49:525–40.
460 Eurocode 8. (2005). “Design of structures for earthquake resistance -Part 2: Bridges.” European Committee for
461 Standardization.
462 Golzan, B., Langlois, S. and Légeron F. (2015). “Simplified design method for energy dissipating devices in
463 retrofitting of seismically isolated bridges.” CSCE 2015 Annual Conference; Regina, Saskatchewan. May 27-30
464 Hwang, J. S., Chiou, J. M., Sheng, L. H., and Gates, J. H. (1996). “A refined model for base-isolated bridges with
465 bi-linear hysteretic bearings.” Earthquake Spectra, Vol. 12, No. 2, pp.245-272.
466 Jangid R.S. and Kelly J.M. (2001). “Base isolation for near-fault motions.” Journal of Earthquake Engineering and
467 Structural Dynamics, 30:691-707.
468 Jara, M., Cass, J.R. (2006). “A direct displacement-based method for the seismic design of bridges on bi-linear
469 isolation devices.” Engineering Structures, 28 869–879
470 Kelley J.M. (1999). “The Role of Damping in Seismic Isolation.” Journal of Earthquake Engineering and Structural
471 Dynamics; 28:3–20.

Kwag, S., Ok, S.Y., (2012). “Robust Design of Seismic Isolation System using Constrained Multi-objective Optimization Technique”. KSCE Journal of Civil Engineering, 17(5):1051-1063.

Lamarche, C. P., Bonelli, A., Bursi, O. S., and Tremblay, R. (2009). “A Rosenbrock-W method for real time dynamic substructuring and pseudo-dynamic testing.” Journal of Earthquake Engineering and Structural Dynamics, 8(9), 1071–1092.

Maleki S. and Bagheri S. (2010), “Pipe Damper, Part II: Application to Bridges,” Journal of Constructional Steel Research, 66(8): 1096−1106.

Mishra, S., Gur, S., Roy, K., and Chakraborty, S. (2015). "Response of Bridges Isolated by Shape Memory–Alloy Rubber Bearing." Journal of Bridge Engineering, 10.1061/(ASCE)BE.1943-5592.0000837, 04015071.

Moreschi, L. M., and Singh, M. P. (2003). “Design of yielding metallic and friction dampers for optimal seismic performance.” Journal of Earthquake Engineering and Structural Dynamics, 32:1291–1311.

Naeim, F., and Kelly, J. M. (1999). Design of seismic isolated structures: from theory to practice, John Wiley, New York.

Oh, S.H., Song, S.H., Lee, S.H., and Kim, H.J. (2012). “Seismic Response of Base Isolating Systems with U-shaped Hysteretic Dampers.” International Journal of Steel Structures. Vol 12, No 2, 285-298.

Pan P., Yan H., Wang T., Xu P. and Xie, Q. (2014), “Development of steel dampers for bridges to allow large displacement through a vertical free mechanism” Earthq Eng & Eng Vib (2014) 13: 375-388

Park, Y. J., Wen, Y. K. and Ang, A. H.-S. (1986), “Random vibration of hysteretic systems under bi-directional ground motions.” Journal of Earthquake Engineering and Structural Dynamics, 14: 543–557.

Priestley, M.J.N., Seible, F., and Calvi, G.M. (1996). “Seismic design and retrofit of bridges.” John Wiley & Sons, New York, USA. P.179

Roesset, J.M., Whitman, R.V., Dobry, R. (1973). “Modal analysis for structures with foundation interaction.” Journal of the Structural Division, ASCE; 99(ST3): 399–416.

Skinner, R. I., Beck, R. I., and Bycroft, G. N., (1975). “A Practical System for Isolating Structures from Earthquake Attack,” Journal of Earthquake Engineering and Structural Dynamics, 13 (3). pp. 297-309.

Skinner, R. I., Robinson, W. H., and McVerry, G. H. (1993). “An Introduction to Seismic Isolation.” John Wiley & Sons, New York, USA.

Stiemer, S. F., Godden, W. G., and Kelly, J. M., (1981). “Experimental Behavior of a Spatial Piping System with Steel Energy Absorbers Subjected to Simulated Differential Seismic Input,” Report No. UCB/EERC 81-09, Earthquake Engineering Research Center, University of California at Berkeley, Berkeley, CA.

Suzuki, K., Watanabe, A., and Saeki, E. (2005). “Development of U-shaped steel damper for seismic isolation system.” Nippon Steel Technical Report No. 92, Japan.

Zhang, R. H. and Soong, T. T., (1992). “Seismic Design of Viscoelastic Dampers for Structural Applications,” Journal of Structural Engineering, 118(5), 1375-1392.